Editors' Suggestion

Measurement, modeling, and correction of decapolar Hamiltonian terms in the LHC

Maël Le Garrec*
CERN, Geneva, Switzerland,
CNRS/IN2P3-LAPP, Annecy-le-Vieux, France;
and Goethe-Universität, Frankfurt, Germany

Ewen Hamish Maclean, Félix Simon Carlier, and Rogelio Tomás
CERN, Geneva, Switzerland

(Received 4 December 2025; accepted 29 September 2026; published 5 November 2026)

Understanding and mitigating high-order nonlinearities is essential for ensuring long-term beam storage in high-energy colliders. The stability of particles at the Large Hadron Collider (LHC) is indeed strongly influenced by nonlinear effects, particularly at injection energy where the beam occupies a large fraction of the vacuum chamber. Among these effects, third-order chromaticity, primarily driven by decapolar fields, limits dynamic aperture and beam lifetime. Despite corrections based on magnetic measurements and model predictions, a discrepancy remains between the measured and expected third-order chromaticity, indicating the presence of residual decapolar components. In this study, the decapolar fields in the LHC at injection energy are investigated and their impact on beam dynamics assessed. Chromatic amplitude detuning and decapolar resonance driving terms are directly measured for the first time, using forced oscillations driven by an ac dipole. These measurements provide new insights into the source and impact of decapolar fields in the LHC and indicate that refined correction strategies could enhance beam lifetime, particularly for high-brightness operation in future runs.

DOI: 10.1103/v1pv-svvx

I. INTRODUCTION

The Large Hadron Collider (LHC) circulates two counterrotating proton beams in separate vacuum chambers, referred to throughout this paper as *beam 1*, traveling clockwise, and *beam 2*, traveling counterclockwise [1]. It is equipped with 1232 main dipoles, organized in cells as depicted in Fig. 1. These cells are placed in the *arcs*, as opposed to the straight sections where beam instrumentation, rf cavities, collimation, and detectors are located. Due to the coil geometry and manufacturing tolerances, these dipoles feature magnetic field errors. Beam-based measurements have been performed since Run 1 (2010) to better characterize the decapolar components, primarily through chromaticity measurements [2–4]. The third-order nonlinear chromaticity, Q''', mostly driven by decapolar errors in the main dipoles, is corrected using decapolar correctors, known as spool-pieces *MCD*. These correctors are initially powered according to the measured field errors of the main dipoles.

Repeated measurements at injection energy have shown that this correction is not effective, as a consistent discrepancy appears from its expected value from simulations, as shown in Table I. Figure 2 illustrates this discrepancy between the supposedly corrected machine and the corrected model; the lower-order chromaticities are matched to measured Q' and Q'' to allow for a better comparison of the third order.

The magnetic model of the LHC's magnets, FiDeL [5], is used to predict the higher-order field errors at various energies. Particularly, it is used in operation to compute corrections for the decapolar fields created by the main dipoles at injection energy. The operational corrections are based on this magnetic model, hence, the residual Q''' value is expected to be small, which is, however, not the case.

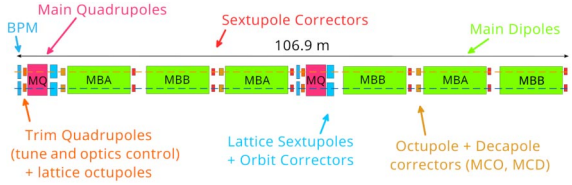


FIG. 1. Schematic view of an LHC arc cell [1].

*Contact author: mael.le.garrec@cern.ch

Published by the American Physical Society under the terms of the Creative Commons Attribution 4.0 International license. Further distribution of this work must maintain attribution to the author(s) and the published article's title, journal citation, and DOI.

TABLE I. Q''' values for the measured corrected machine, in April 2022, and the model, for both uncorrected and corrected errors.

	Q'''_x [10^6]	Q'''_y [10^6]
Uncorrected model	6.97	−4.33
Corrected model	−0.77	0.00
Measurement	-3.37 ± 0.04	1.62 ± 0.05

While the study of nonlinear chromaticity has proven valuable in identifying the existence of this discrepancy, it does not yet permit alone to understand its exact origins. Additional measurements were performed in an effort to gain deeper insights. *Bare chromaticity* is the chromaticity measured with the octupolar and decapolar correctors deactivated, isolating the contribution of the main dipoles from that of the correctors. While chromaticity itself is a routine measurement in any circular accelerator, this bare configuration had not been measured at the LHC in several years, as the correctors were assumed to be performing as expected. *Chromatic amplitude detuning*, which evaluates how the tune varies with both the beam's action and the momentum offset, had on the other hand never been measured at the LHC before the present work. Because its dependence on both action and momentum differs from that of chromaticity, it can distinguish purely momentum-dependent effects, such as higher-order dispersion, from genuine decapolar field errors.

Direct measurements of decapolar resonance driving terms (RDTs) were conducted for the first time in the LHC at injection energy. These high-order RDTs, which drive resonances near the LHC working point, have also been corrected for the first time within this work, using a response matrix-based approach. Lower-order multipoles, such as sextupoles and octupoles, were found to contribute significantly to the decapolar RDTs. Their effects are thoroughly studied, as they are expected to strongly impact the dynamic aperture [6] at injection energy. Nonlinear

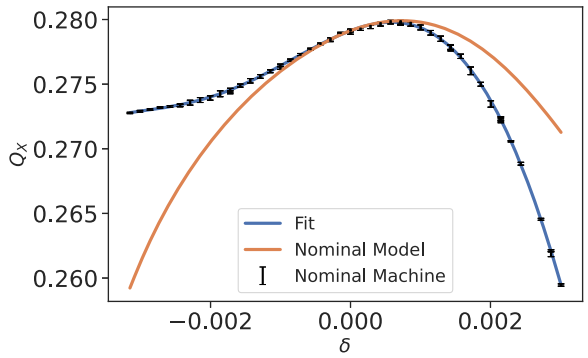


FIG. 2. Measured and simulated tune at various momentum offsets δ in 2022, with application of the nominal decapolar corrections. It can be seen that Q''' is not well corrected in practice.

fields have been studied in detail in various machines, such as RHIC [7,8], the Tevatron [9], and the LHC [1,8,10–13], in which the dodecapolar fields are of particular interest at top energy [11]. While lower-order field errors in the LHC are generally well understood and controlled, this is not the case for higher-order errors such as decapoles and beyond. Precise control of these higher-order nonlinearities is expected to be crucial for future accelerators and colliders, where field corrections will play a large role in maintaining an optimal dynamic aperture [11,14–16]. Addressing this gap is essential for improving higher-order corrections in the LHC and preparing for the challenges of its next upgrade, the HL-LHC, where the integrated luminosity is expected to be increased by a factor of 10 [17].

This paper is organized as follows. Section II presents the measurements of the nonlinear chromaticity versus decapole corrector strength. Section III shows the results of bare chromaticity measurements, without any decapolar corrections applied. Section IV presents the first chromatic amplitude detuning measurements and their implications for understanding the decapolar field discrepancies. The identified source of the discrepancy is detailed in Sec. V. The study of RDTs, particularly the f_{1004} term, is presented in Sec. VI, where the contributions from lower-order multipoles are also explored. Finally, the impact of these findings on beam stability and dynamic aperture is discussed.

A. Theoretical formulation

The integrated strength for a multipole of order n, following the convention used by MAD-X/PTC [18], is given by the following:

$$K_n = \frac{L}{B\rho}\frac{\partial^n B_y}{\partial x^n}, \tag{1}$$

where L is the length of the magnetic element, $B\rho$ the magnetic rigidity, and B_y the vertical component of the magnetic field. The tune variation, $\Delta Q_{x,y}$, versus the relative momentum offset, δ, is referred to as chromaticity,

$$\Delta Q(\delta) = Q'\delta + \frac{1}{2!}Q''\delta^2 + \frac{1}{3!}Q'''\delta^3 + \mathcal{O}(\delta^4). \tag{2}$$

Experimentally, δ is varied via the rf frequency f_{rf}, related through the momentum compaction factor α_c, neglecting the Lorentz factor γ [19],

$$\delta = -\frac{1}{\alpha_c}\cdot\frac{\Delta f_{\mathrm{rf}}}{f_{\mathrm{rf}}}. \tag{3}$$

Its variation with the action, $J_{x,y}$, is called amplitude detuning. Chromatic amplitude detuning is the tune variation with both action and momentum, defined to leading order as follows:

$$\Delta Q(J_x, J_y, \delta) = \frac{\partial^2 Q}{\partial J_x \partial \delta} J_x \delta + \frac{\partial^2 Q}{\partial J_y \partial \delta} J_y \delta. \tag{4}$$

The coefficients with the second derivatives depend linearly on the decapolar component, K_5, quadratically on the β-functions, and linearly on the horizontal dispersion, D_x. Throughout this paper, the coefficients in which the tune and the action refer to the same plane, $\partial^2 Q_x/\partial J_x \partial \delta$ and $\partial^2 Q_y/\partial J_y \partial \delta$, are called *direct* terms, while those coupling the two planes, $\partial^2 Q_x/\partial J_y \partial \delta$ and $\partial^2 Q_y/\partial J_x \partial \delta$, are called *cross* terms. For a single source of length L, we have

$$\begin{aligned}
\frac{\partial^2 Q_x}{\partial J_x \partial \delta} &= \frac{1}{16\pi} K_5 L \beta_x^2 D_x, \\
\frac{\partial^2 Q_y}{\partial J_y \partial \delta} &= \frac{1}{16\pi} K_5 L \beta_y^2 D_x, \\
\frac{\partial^2 Q_x}{\partial J_y \partial \delta} &= \frac{\partial^2 Q_y}{\partial J_x \partial \delta} = -\frac{1}{8\pi} K_5 L \beta_x \beta_y D_x, \\
\frac{\partial^3 Q_x}{\partial \delta^3} &= \frac{1}{4\pi} K_5 L \beta_x D_x^3, \\
\frac{\partial^3 Q_y}{\partial \delta^3} &= -\frac{1}{4\pi} K_5 L \beta_y D_x^3.
\end{aligned} \tag{5}$$

The dynamics of a particle beam in a circular accelerator can be described by *transfer maps*. The symplectic *one-turn map*, $\mathcal{M}$, including N nonlinear elements is defined as [20],

$$\mathcal{M} = e^{:h_N:} \cdot e^{:h_{N-1}:} \cdots e^{:h_1:} \cdot \mathcal{R}, \tag{6}$$

where $\mathcal{R}$ describes the linear motion over one turn and each $e^{:h_i:}$ is the Lie transformation associated with the ith nonlinear element of the machine, h_i being its Hamiltonian expressed in the eigencoordinates at the longitudinal position of that element [20,21]. The one-turn map is thus written as a succession of nonlinear kicks acting on the linear motion. Via the Baker-Campbell-Hausdorff (BCH) theorem [22,23], these Lie transformations can be combined as

$$e^{:h_1:} \cdot e^{:h_2:} = e^{:h:}, \tag{7}$$

with,

$$\begin{aligned}
h = {} & h_1 + h_2 && \Rightarrow 1^{\text{st}} \text{ order} \\
& + \frac{1}{2}[h_1, h_2] && \Rightarrow 2^{\text{nd}} \text{ order} \\
& + \frac{1}{12}[h_1, [h_1, h_2]] - \frac{1}{12}[h_2, [h_1, h_2]] && \Rightarrow 3^{\text{rd}} \text{ order} \\
& + \cdots.
\end{aligned} \tag{8}$$

Higher orders are described in [23]. In most cases, nonlinear perturbations are small and the above series converges quickly and only the first order of Eq. (8) is used [24]. However, this paper will show that considering higher orders of the BCH expansion is important in the LHC; explicit derivations of representative cases, where decapolarlike terms are generated by combinations of lower-order multipoles, are given in the Appendix.

After N turns, the normalized transverse coordinates are given by [25]

$$\begin{aligned}
(x - ip_x)(N) &= \sqrt{2I_x} e^{i(2\pi Q_x N + \phi_{x_0})} - 2i \sum_{jklm} j f_{jklm} (2I_x)^{\frac{j+k-1}{2}} (2I_y)^{\frac{l+m}{2}} e^{i[(1-j+k)(2\pi Q_x N + \phi_{x_0}) + (m-l)(2\pi Q_y N + \phi_{y_0})]}, \\
(y - ip_y)(N) &= \sqrt{2I_y} e^{i(2\pi Q_y N + \phi_{y_0})} - 2i \sum_{jklm} l f_{jklm} (2I_x)^{\frac{j+k}{2}} (2I_y)^{\frac{l+m-1}{2}} e^{i[(k-j)(2\pi Q_x N + \phi_{x_0}) + (1-l+m)(2\pi Q_y N + \phi_{y_0})]},
\end{aligned} \tag{9}$$

where the f_{jklm} are the coefficients of the generating function of the normal-form transformation, ϕ_{x_0,y_0} the initial phases and $I_{x,y}$ the actions. The summation expands over all the combinations of j, k, l, and m with order $j + k + l + m \leq n$. Equation (9) is kept to first order in the f_{jklm}, which is sufficient here: each f_{jklm} appears as a single spectral line of the turn-by-turn motion, with amplitude directly proportional to it, from which it is measured [26]. Higher orders would add only weaker combination lines and small corrections to these amplitudes, so that each f_{jklm} being read from its leading line, the first-order relation is sufficient. Which resonances appear is set by the nonvanishing Hamiltonian terms h_{jklm} [21,25,27]; capturing those generated by combinations of lower-order multipoles, such as the decapolarlike terms studied here, requires carrying the BCH expansion of Eq. (8) to third order. The f_{jklm} are related to the Hamiltonian terms h_{jklm} by

$$f_{jklm} = \frac{h_{jklm}}{1 - e^{i2\pi[(j-k)Q_x + (l-m)Q_y]}}, \tag{10}$$

where h_{jklm} can be approximated as a summation over the nonlinear elements in the lattice [21].

Historically, it is the Hamiltonian coefficients h_{jklm} that are termed resonance driving terms, the f_{jklm} being the coefficients of the generating function [25,27]. In the context of beam-based measurements, where f_{jklm} is the quantity directly accessible from the spectral lines of turn-by-turn data, the term has come to be applied to the f_{jklm} as well. This latter convention is the one followed here: from this point on, the f_{jklm} are the quantities referred to as the resonance driving terms, and the h_{jklm} as the Hamiltonian terms.

Equations (9) and (10) describe the *free* motion of a particle, oscillating at the natural tunes $Q_{x,y}$. In the LHC, however, RDTs and chromatic amplitude detuning are measured by driving the beam to a finite action with an ac dipole, exciting coherent oscillations at driving tunes $Q_{x,\mathrm{ac}}, Q_{y,\mathrm{ac}}$ distinct from the natural tunes [26]. The measured quantity is therefore not the *free* RDT f_{jklm} of Eq. (10), but a *forced* counterpart f^{ac}_{jklm}. In the presence of the ac dipole the same spectral decomposition holds with the natural tunes replaced by the driving ones [26]: the spectral lines of Eq. (11) are then observed at the corresponding combinations of the ac-dipole tunes $Q_{x,\mathrm{ac}}, Q_{y,\mathrm{ac}}$, and their amplitudes [Eq. (12)] scale with the forced actions and with $|f^{\mathrm{ac}}_{jklm}|$. The forced RDT is thus defined operationally as the quantity extracted from this forced spectrum, identically in measurement and in tracking. Unlike RDTs and chromatic amplitude detuning, the chromaticity terms Q', Q'', Q''' of Eq. (2) are obtained at zero transverse amplitude from a momentum scan and do not involve the ac dipole.

Resonance driving terms affect the transverse motion of particles. As a result, performing a Fourier transform on the turn-by-turn beam signal reveals spectral lines associated with specific RDTs. Each forced RDT f^{ac}_{jklm} may appear in the frequency spectrum of the horizontal plane, the vertical plane, or both, at harmonics of the driving tunes $Q_{x,\mathrm{ac}}$ and $Q_{y,\mathrm{ac}}$. The following expression indicates the positions of these lines in the horizontal (H_{jklm}) and vertical (V_{jklm}) spectra,

$$\begin{aligned} H_{jklm} &\quad \text{at } (1-j+k)Q_{x,\mathrm{ac}} + (m-l)Q_{y,\mathrm{ac}}\,, \qquad j \neq 0 \\ V_{jklm} &\quad \text{at } (k-j)Q_{x,\mathrm{ac}} + (1-l+m)Q_{y,\mathrm{ac}}, \qquad l \neq 0. \end{aligned} \tag{11}$$

The amplitude of each spectral line depends on the forced actions $I_{x,y}$ and the amplitude of the forced RDT [25,26] as follows,

$$\begin{aligned} |H_{f_{jklm}}| &= 2j(2I_x)^{\frac{j+k-1}{2}}(2I_y)^{\frac{l+m}{2}}|f^{\mathrm{ac}}_{jklm}|, \\ |V_{f_{jklm}}| &= 2l(2I_x)^{\frac{j+k}{2}}(2I_y)^{\frac{l+m-1}{2}}|f^{\mathrm{ac}}_{jklm}|. \end{aligned} \tag{12}$$

The RDT is then computed via a fit of the spectral line amplitude versus actions. All RDT and chromatic amplitude detuning measurements presented in this paper are obtained this way, using ac dipoles with varying excitation amplitude [28,29]. Simulations are consistently performed with a matching ac-dipole excitation, so that every comparison between measurement and model in this paper is made between forced quantities. As all RDTs reported in the following are forced, the superscript is omitted hereafter and f_{jklm} denotes the forced RDT.

The free machine, however, only exhibits *free* RDTs, which are the quantities ultimately relevant for the long-term stability of stored beams. No general analytic mapping between forced and free RDTs is presently available for arbitrary multipole order; establishing one is the subject of ongoing work [24,30]. Correcting the forced RDT is therefore taken in this paper as a proxy for correcting the underlying free RDT. The validity of this assumption is supported *a posteriori* by the beam lifetime measurements of Sec. VI, a free-motion observable, which confirm that the forced-RDT-based correction translates into a measurable benefit for the free beam.

II. CONFIRMING THE RESPONSE OF DECAPOLAR CORRECTORS

By analyzing the actual response of the tune Q versus applied current in the decapolar correctors, it is possible to determine whether the source of the Q''' discrepancy originates from a miscalibration of the decapolar correctors or not. The MCD correctors are specific to each beam and are placed after every second dipole, totaling 1232 for both beams [31]. MCDs are nested with octupolar correctors, *MCOs*. The pair of these correctors is often referred to as *MCDO*. There is a total of 16 MCD circuits to power the correctors of both beams, corresponding to one per arc and per beam. Figure 3 shows a picture of decapoles before installation.

One possible source of unwanted fields could be crosstalk between *MCOs* and *MCDs* as they are nested [31]. During Run 3's commissioning, routine measurements and corrections of Q'' and Q''' have been established, which provide a valuable opportunity to analyze the response of the *MCDs*. Throughout this paper, Q', Q'', and Q''' are obtained from a polynomial fit of the measured tune versus δ to Eq. (2); the quoted uncertainties on these terms are obtained from the covariance matrix of the fit.

Figure 4 shows the tune variation versus momentum offset δ measured in 2022 with the nominal FiDeL corrections and with further corrections computed online, aimed at correcting Q'' and Q'''.

The nominal and corrected Q''' values are shown in Table II, with the shift in Q''' for each beam and axis. Good agreement between measurements and simulations is

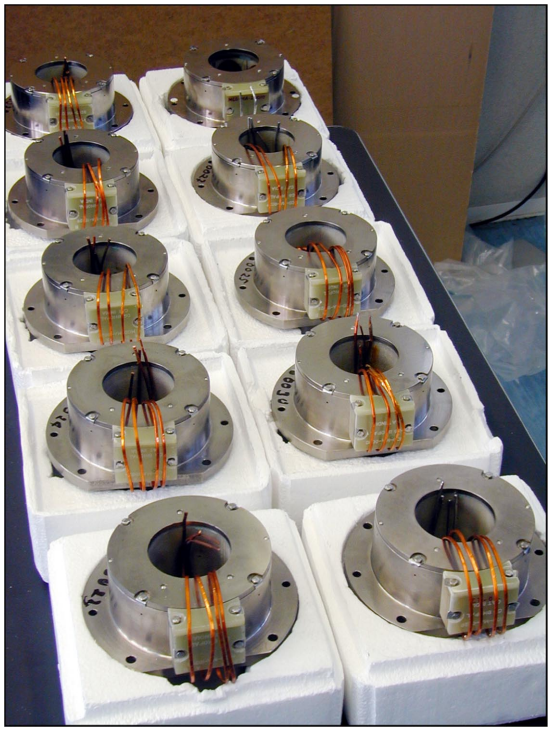


FIG. 3. Decapoles before installation, being inspected after manufacturing [32].

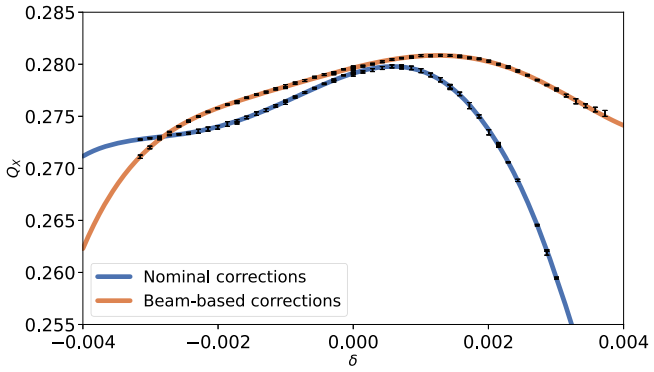


FIG. 4. Chromaticity of the horizontal plane of beam 1 during Run 3's commissioning, with nominal corrections based on the magnetic model and further corrections.

observed for the Q''' shift. This confirms that the decapole correctors are working as intended.

III. FIRST MEASUREMENT OF BARE CHROMATICITY AT THE LHC

Measurements of the bare machine, without any octupolar or decapolar correctors powered, further help rule out potential crosstalk between the octupolar and decapolar correctors and offer a direct assessment of the magnetic model. The obtained results are presented in Fig. 5.

TABLE II. Third-order chromaticity *measured* during Run 3 commissioning, under two correction schemes: the nominal corrections, based on the magnetic model, and the additional beam-based corrections, aimed at further correcting Q'' and Q'''. The resulting shift in Q''' between the two schemes is compared, for both measurement and simulation, in the right-hand table.

	$Q'''[10^6]$		$\Delta Q'''[10^6]$	
Plane	Nominal	Beam-based	Measurement	Simulation
Beam 1				
X	-3.36 ± 0.04	-1.02 ± 0.03	2.3 ± 0.1	2.5
Y	1.62 ± 0.05	0.12 ± 0.02	-1.5 ± 0.1	-1.4
Beam 2				
X	-2.72 ± 0.08	-0.64 ± 0.03	2.1 ± 0.1	2.5
Y	1.54 ± 0.06	0.14 ± 0.03	-1.4 ± 0.1	-1.4

Simulations have been performed with MAD-X and PTC [33] including field errors from FiDeL, from normal sextupole to decahexapole. The expected Q''' values are presented in Table III and compared to the measured ones along with the ratio between the two.

The discrepancy between measurements and simulations persists even with the correctors turned off, implying that the discrepancy may come from the LHC's main magnets. These results indicate that the source likely lies in a systematic error of the decapolar components in the magnetic model. However, relying solely on Q''' does not yield a definitive conclusion, as higher-order effects may

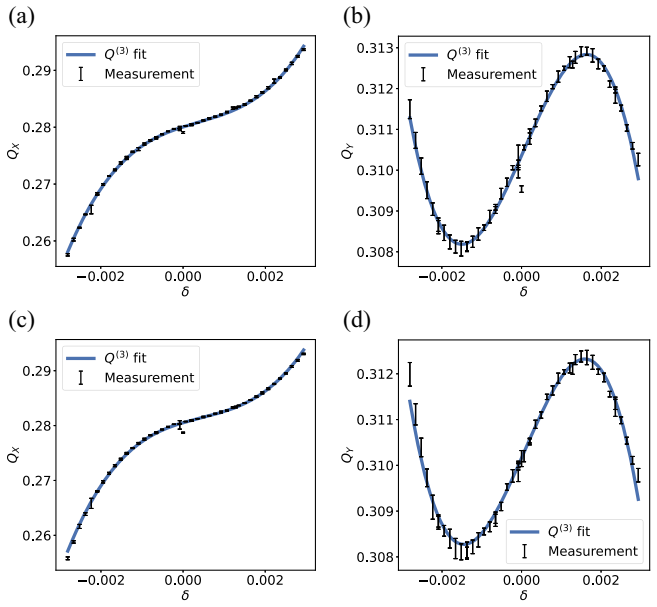


FIG. 5. Tune measurement versus momentum offset δ with octupole and decapole correctors powered off. The fit includes all orders up to the third. (a) Q_x beam 1, (b) Q_y beam 1, (c) Q_x beam 2, and (d) Q_y beam 2.

TABLE III. Measured and simulated third-order chromaticity with octupole and decapole correctors turned off. The simulations include field errors from normal sextupoles to decahexapoles.

Quantity	Measured $[10^6]$	Simulated $[10^6]$	Ratio
Beam 1			
Q_x'''	2.95 ± 0.04	6.94 ± 0.02	0.43 ± 0.01
Q_y'''	-1.82 ± 0.04	-4.29 ± 0.01	0.42 ± 0.01
Beam 2			
Q_x'''	3.06 ± 0.07	7.03 ± 0.02	0.44 ± 0.01
Q_y'''	-1.72 ± 0.02	-4.27 ± 0.01	0.42 ± 0.01

contribute [19,34]. Nonlinear dispersion, via its second order, could indeed introduce some Q''' with octupolar fields. The nonlinear momentum compaction factor may also have an impact with the momentum offset reconstruction. Resolving this will require additional observables; one of which, the chromatic amplitude detuning, is used in the next section.

IV. FIRST MEASUREMENT OF CHROMATIC AMPLITUDE DETUNING AT THE LHC

While the K_5 dependence of the chromatic amplitude detuning is identical to that of Q''', the β and D_x dependencies differ significantly. In the presence of a systematic error in the main dipoles, one would expect similar ratios between measurements and simulations for this observable as for $Q'''_{x,y}$. If the errors were to originate from the straight sections, the ratios would differ. The action-dependent terms can be measured at various momentum offsets by varying the rf frequency and exciting the beam to high amplitudes, which in the LHC is typically achieved using an ac dipole [35,36], whose strength can be gradually increased. Such a measurement was performed during a beam test with octupole and decapole correctors turned off to probe the bare machine, at relative momentum offsets of $\delta = -0.001$ and $\delta = 0.001$. The terms $\frac{\partial^2 Q_x}{\partial J_y \partial \delta}$ and $\frac{\partial^2 Q_y}{\partial J_y \partial \delta}$ for beam 2 were successfully measured for the first time in the LHC. Figures 6(a) and 6(b) show a fit of the amplitude detuning, $Q_{x,y}$ versus $2J_y$, at two different momentum offsets. Expected shifts from MADX-PTC simulations that include field errors ranging from sextupoles to decahexapoles (b_3 to b_8 and a_4 to a_8) are also shown as a comparison. Free amplitude detuning is simulated in PTC and adapted to its forced value to allow comparisons to measurements with ac dipoles, as the correction coefficients for the direct and cross terms differ [36,37].

The values for the amplitude detuning at discrete momentum offsets and ratios of measurement to model can be found in Table IV, while Table V shows the fitted

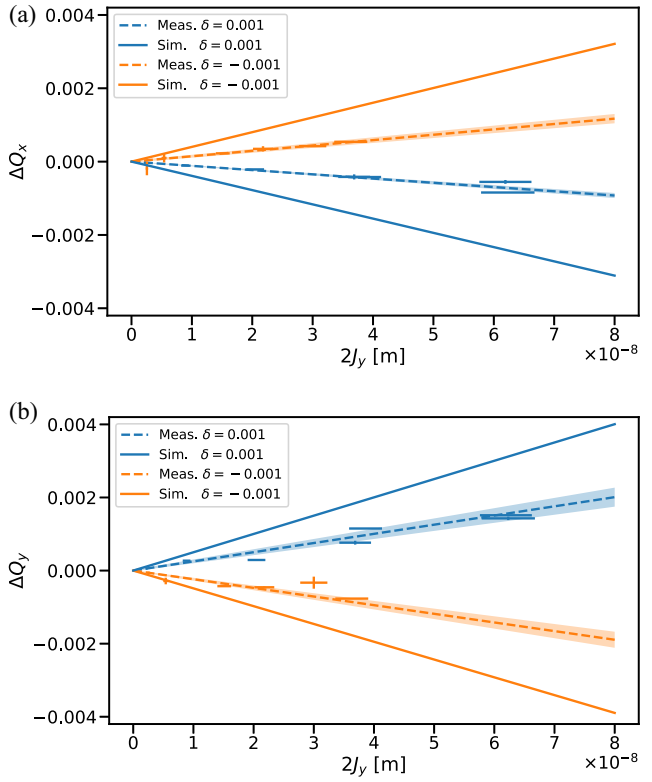


FIG. 6. Measured and simulated forced tune shifts due to a change of action via an ac dipole at two different momentum offsets in beam 2. Fits to the measured data are also shown. (a) Horizontal tune shift depending on the vertical action (b) vertical tune shift depending on the vertical action.

chromatic amplitude detuning. The observed ratios for the chromatic amplitude detuning are quite similar, while not equal, to those of the bare chromaticity. This similarity suggests that most of the decapolar deviations should lie within the main dipoles, with measurements showing values between one third and one half of those predicted by the magnetic model.

TABLE IV. Comparison of measured and simulated forced amplitude detuning terms via PTC, at two discrete momentum offsets for beam 2. Simulations include errors from normal sextupole to decahexapole and from skew octupole to decahexapole.

Type	$\frac{\partial Q_x}{2\partial J_y}$ $[10^4$ m$^{-1}]$	$\frac{\partial Q_y}{2\partial J_y}$ $[10^4$ m$^{-1}]$
$\delta = +0.001$		
Measurement	-1.16 ± 0.08	1.26 ± 0.15
Simulation	-3.82 ± 0.01	2.47 ± 0.01
Ratio	0.30 ± 0.02	0.51 ± 0.06
$\delta = -0.001$		
Measurement	1.47 ± 0.12	-1.18 ± 0.13
Simulation	3.92 ± 0.01	-2.41 ± 0.01
Ratio	0.38 ± 0.03	0.49 ± 0.05

TABLE V. Comparison of measured and simulated forced chromatic amplitude detuning values for beam 2, obtained from fitting amplitude detuning terms versus δ from Table IV.

Type	$\frac{\partial^2 Q_x}{2\partial J_y \partial \delta}$ [10^6 m^{-1}]	$\frac{\partial^2 Q_y}{2\partial J_y \partial \delta}$ [10^6 m^{-1}]
Measurement	-13.2 ± 0.7	12.2 ± 1.0
Simulation	-38.7 ± 0.1	24.4 ± 0.1
Ratio	0.34 ± 0.02	0.50 ± 0.04

V. ACCOUNTING FOR DECAY

Magnetic decay in superconducting magnets stems from field changes in the strands caused by current redistribution in the superconducting cables. Decay has been shown to be strongly dependent on the magnet powering history [38,39]. This happens, for example, when ramping down from an energy of 6.8 TeV to 0 and then going back to injection energy at 450 GeV. Some components of the magnetic field will persist and gradually change over time until they reach their final values.

While the sextupolar b_3 decay is accounted for during operations, a review of the FiDeL model revealed that the decapolar component b_5 has not been similarly considered. To date, all beam dynamics studies in the LHC have relied on the same set of magnetic measurement error tables, neglecting any decapolar decay. The b_5 component used in simulations is shown in Fig. 7, where the average b_5 at injection energy is about 1.13 ± 0.56 units.

However, during LHC construction, magnetic measurements were actually performed on a representative set of main dipoles, allowing the b_5 decay to be quantified. For reference, decay measurements of a selection of main dipoles over time are illustrated in Fig. 8, where each dot represents a measured dipole. Table VI shows the decay expected at injection energy after a typical cycle of machine operation. From this table, it is clear that decay accounts for a large part of the b_5 at injection. About 40% of the total b_5 at injection in the main dipoles can indeed be attributed to the decay.

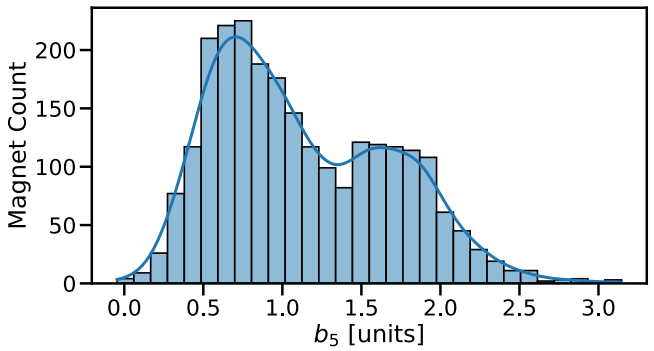


FIG. 7. Distribution of the decapolar component b_5 in the main dipoles at injection energy.

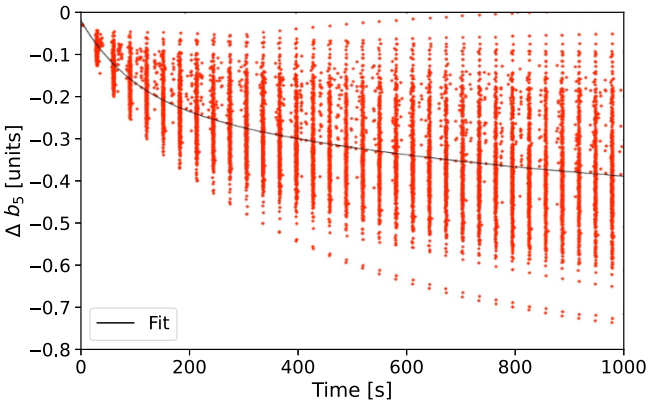


FIG. 8. Measured decapolar field in LHC's main dipoles at injection energy with respect to time, highlighting its decay [40].

Only the first row of Table VI, at 17 min, was directly measured, with a dipole-to-dipole spread of $\sigma = 0.11$ units; all later times are obtained by extrapolating the fitted decay curve well beyond the 17-min measurement window. As this extrapolation uncertainty is not quantified in [40], the measured spread of 0.11 units is taken as a lower bound on the uncertainty of the extrapolated values.

Unfortunately, individual magnet measurements conducted more than 15 years ago could not be recovered, as only a summary table and plots were available. As a result, the b_5 decay in the simulations is implemented as the average decay from all the probed magnets and applied uniformly to all main dipoles. In the following simulations, each main dipole has its b_5 component reduced by 0.47 ± 0.11 units, where the quoted uncertainty is the lower bound discussed above.

A. Chromaticity

As shown in the previous sections, and in particular in Table III, a discrepancy was observed between measurements and simulations of the third-order chromaticity Q'''. New simulations of the bare machine have hence been conducted to evaluate the effect of this decay on chromaticity. Table VII compares simulations with and without the decay of the b_5 component for beam 1, similar results are seen for beam 2.

TABLE VI. Decay of the b_5 component after injection for long time periods [40].

Time (min)	Δb_5
17	−0.38
33	−0.44
50	−0.46
67	−0.47
83	−0.47
167	−0.47

TABLE VII. Comparison of Q_x''' and Q_y''' for beam 1 with and without decay of the b_5 component of the main dipoles at injection energy without corrections. Included fields errors range from normal and skew sextupoles ($n = 3$) to icosapoles ($n = 10$). The uncertainty on the $\Delta b_5 = -0.47$ row is dominated by the propagated decay uncertainty.

Condition	$Q_x'''[10^6]$	$Q_y'''[10^6]$
No decay	6.93 ± 0.04	-4.32 ± 0.02
$\Delta b_5 = -0.47$	4.05 ± 0.67	-2.54 ± 0.42

For every quantity below that depends on the decay, the sensitivity to Δb_5 is estimated as the finite difference between the simulation without decay and the simulation with the nominal $\Delta b_5 = -0.47$ applied. This sensitivity, multiplied by the ± 0.11 uncertainty on Δb_5 obtained above, is added in quadrature to the original simulation uncertainty, and dominates the resulting error bars throughout this section.

Implementing the decay of the b_5 component of the main dipoles in the simulations has significantly reduced the discrepancy between beam-based measurements and the magnetic model. While the overall ratio between measurements and simulations across all planes and beams was previously close to 0.4, it is now approximately 0.7 ± 0.1. Using the results obtained from the bare chromaticity measurement in Table III and updating the simulation column with the newly simulated decay provides a more accurate description of the magnetic model, as shown in Table VIII.

B. Chromatic amplitude detuning

Similar to chromaticity, new simulations have been conducted for chromatic amplitude detuning. Table IX gives an overview of the newly computed amplitude detuning values at discrete momentum offsets and the related ratios relative to the measurements. Table X gives the final chromatic amplitude detuning values with the ratios. A difference in the quality of the agreement can be observed between the direct term $\frac{\partial^2 Q_y}{2\partial J_y \partial \delta}$ and the cross term $\frac{\partial^2 Q_x}{2\partial J_y \partial \delta}$. This may arise from the implementation of decay, which only considers the average b_5 across all dipoles and may not fully capture the individual variations. Nevertheless, both terms now demonstrate a better agreement with the model deviating by $45 \pm 8\%$ and $17 \pm 14\%$, not far from the 30% deviation seen with chromaticity. Given the size of the propagated decay uncertainty, the remaining deviation on the cross term is only marginally significant. Smaller, yet unidentified, errors are therefore likely still present in the machine. In addition to decay, hysteresis in the magnetic steel surrounding the superconducting coils is another history-dependent effect that could in principle contribute, as observed in other colliders [41]. The precycle performed before injection in the LHC makes the main-dipole hysteresis largely reproducible, so it is not expected to be a dominant source; a small residual, powering-history-dependent contribution can nonetheless not be entirely excluded.

TABLE VIII. Measured and simulated third-order chromaticity with octupole and decapole correctors turned off. The simulations include field errors from normal and skew sextupoles to icosapoles ($n = 3$ to $n = 10$). The b_5 component in simulations has been updated to include decay.

Quantity	Measured $[10^6]$	Simulated $[10^6]$	Ratio
Beam 1			
Q_x'''	2.95 ± 0.04	4.05 ± 0.67	0.73 ± 0.12
Q_y'''	-1.82 ± 0.04	-2.54 ± 0.42	0.72 ± 0.12
Beam 2			
Q_x'''	3.06 ± 0.07	4.27 ± 0.67	0.72 ± 0.11
Q_y'''	-1.72 ± 0.02	-2.55 ± 0.42	0.67 ± 0.11

TABLE IX. Comparison of measured and simulated amplitude detuning terms via PTC, at two discrete momentum offsets. Simulations include errors from normal and skew sextupoles to icosapoles ($n = 3$ to $n = 10$), as well as the decay of the b_5 component of the main dipoles. The simulation uncertainty is dominated by the propagated b_5 decay uncertainty, estimated via the same finite difference as in Table VII.

Type	$\frac{\partial Q_x}{2\partial J_y}[10^4\ \mathrm{m}^{-1}]$	$\frac{\partial Q_y}{2\partial J_y}[10^4\ \mathrm{m}^{-1}]$
$\delta = +0.001$		
Measurement	-1.16 ± 0.08	1.26 ± 0.15
Simulation	-2.35 ± 0.34	1.50 ± 0.23
Ratio	0.49 ± 0.08	0.84 ± 0.16
$\delta = -0.001$		
Measurement	1.47 ± 0.12	-1.18 ± 0.13
Simulation	2.46 ± 0.34	-1.45 ± 0.22
Ratio	0.60 ± 0.10	0.82 ± 0.15

TABLE X. Comparison of measured and simulated forced chromatic amplitude detuning values with and without decay, obtained from fitting amplitude detuning terms versus δ from Tables IV and IX. The uncertainty on the simulation with decay is dominated by the propagated b_5 decay uncertainty, estimated via the finite difference with the no-decay simulation.

Type	$\frac{\partial^2 Q_x}{2\partial J_y \partial \delta}[10^6\ \mathrm{m}^{-1}]$	$\frac{\partial^2 Q_y}{2\partial J_y \partial \delta}[10^6\ \mathrm{m}^{-1}]$
Measurement	-13.2 ± 0.7	12.2 ± 1.0
Simulation without decay	-38.7 ± 0.1	24.4 ± 0.1
Simulation with decay	-24.1 ± 3.4	14.8 ± 2.2
Ratio without decay	0.34 ± 0.02	0.50 ± 0.04
Ratio with decay	0.55 ± 0.08	0.83 ± 0.14

VI. FIRST MEASUREMENTS OF DECAPOLAR RESONANCE DRIVING TERMS

Nonlinear perturbations in the lattice, induced by high-order fields, can excite resonances, leading to potential beam degradation or loss. Powerful observables for their analysis are the RDTs, which quantify the strength of nonlinear resonances and arise naturally in the treatment of nonlinear dynamics using normal form analysis [26].

Decapolar fields have so far been investigated through chromaticity and chromatic amplitude detuning. While the discrepancy in the decapolar fields induced by the main dipoles has been mostly understood, the resonances driven by these fields are not fully characterized, some of which are relevant for LHC operation.

A. Decapolar resonances

Decapoles drive, to first order, 25 RDTs. Of particular interest to LHC operation at injection energy is the RDT f_{1004}, which drives the resonance $1Q_x - 4Q_y$, which is close to the operational working points. Figure 9 shows a frequency map [42] from a simulation including decapolar field errors, where their impact on the beam dynamics is clearly visible. The color map represents the tune diffusion over the course of the simulation, with blue indicating low tune diffusion, while red represents large diffusion, suggesting unstable or chaotic trajectories.

When measuring optics with the ac dipole, this RDT drives a spectral line in the horizontal spectrum at $4Q_{y,\mathrm{ac}}$, whose amplitude depends quadratically on J_y, see Eq. (12). This spectral line, shown in Fig. 10, could be reliably measured with a good signal-to-noise ratio in various configurations of the LHC. Measurements were taken for the first time in the LHC to observe the f_{1004} RDT at injection energy. The most effective working point to measure this RDT was empirically set to $Q_x = 0.28$ and $Q_y = 0.31$ with ac dipole at $Q_{x,\mathrm{ac}} = 0.272$ and $Q_{y,\mathrm{ac}} = 0.322$.

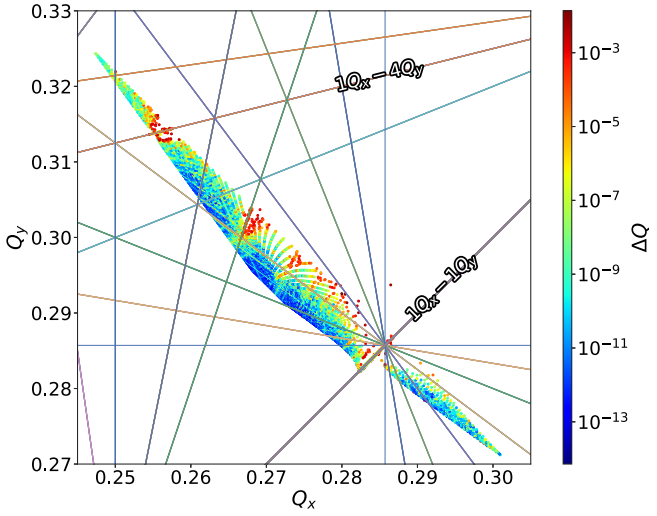


FIG. 9. Frequency map at injection energy, with decapolar field errors and nominal settings for Landau octupoles. The tune shift ΔQ after 20,000 turns is indicated in color. The highlighted resonance $1Q_x - 4Q_y$, excited by decapoles, shows a clear impact on the tune diffusion.

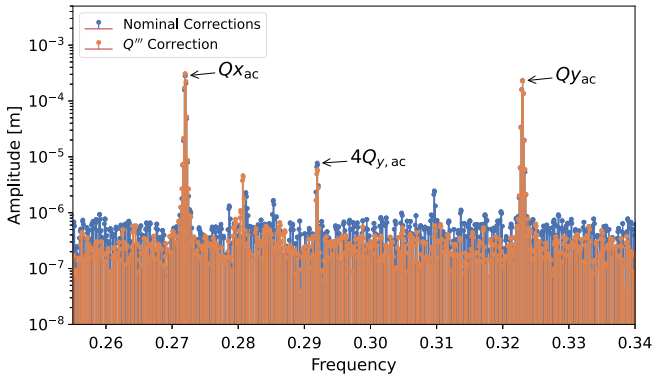


FIG. 10. Horizontal frequency spectrum of turn-by-turn data, with nominal and beam-based corrections for the third-order chromaticity Q'''. The $1Q_x - 4Q_y$ resonance can be seen at $4Q_y$ with different amplitudes for each correction scheme.

B. Measurement and correction

Decapolar fields are usually expected to be the main contributors to the RDT f_{1004}. As such, powering the decapolar correctors is a good way to correct the related resonances. Being linear with the strength of the correctors, the RDT can be corrected via a response matrix.

Measurements were conducted to establish a baseline for the amplitude of the RDT without octupolar or decapolar correctors and with the nominal FiDeL corrections. Such measurement is shown in Fig. 11 for beam 1, similar results are observed for beam 2. It can be observed that the FiDeL corrections, based on the magnetic model and which do not account for the decapolar decay, degrade the RDT.

Corrections were then attempted based on the measurements obtained with the nominal FiDeL settings, after an extended period at injection where the b_5 component of the main dipoles already had saturated. These beam-based

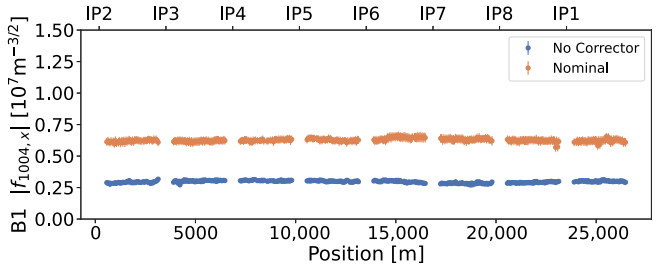


FIG. 11. Amplitude of the forced decapolar RDT f_{1004} measured with and without nominal FiDeL corrections for Q'''. Decay is not included in this correction scheme.

TABLE XI. Strength of decapolar correctors with nominal FiDeL settings and after application of corrections aiming at reducing both the RDT f_{1004} and the third-order chromaticity Q'''. The total value has a direct incidence on Q'''.

Circuit	FiDeL $K_5[\mathrm{m}^{-5}]$	$\Delta K_5[\mathrm{m}^{-5}]$	$K_5[\mathrm{m}^{-5}]$
Beam 1			
RCD.A12B1	−4582	6055	1473
RCD.A23B1	−5106	7	−5099
RCD.A34B1	−4855	3827	−1028
RCD.A45B1	−4577	−4746	−9323
RCD.A56B1	−4125	−4903	−9028
RCD.A67B1	−5166	2961	−2205
RCD.A78B1	−6827	3593	−3234
RCD.A81B1	−5500	2380	−3120
Total	−40,738	9174	−31,564
Beam 2			
RCD.A12B2	−4490	3639	−851
RCD.A23B2	−5155	−1147	−6302
RCD.A34B2	−4825	−1038	−5863
RCD.A45B2	−4619	3986	−633
RCD.A56B2	−4064	2944	−1120
RCD.A67B2	−5066	2357	−2709
RCD.A78B2	−6866	−2952	−9818
RCD.A81B2	−5446	1825	−3621
Total	−40,531	9614	−30,917

corrections were applied on top of the previous FiDeL correction scheme. The strength of the decapolar correctors is shown in Table XI for the FiDeL settings, the delta applied on top, and the final corrector values.

This RDT correction also serves as a partial Q''' correction. To fully correct Q''' approximately requires a strength of $\Delta K_5 = 13{,}000$ distributed among the correctors. Therefore, this new approach reduces Q''' by about 70% compared to the correction fully targeting Q''. The chromatic amplitude detuning terms are also expected to be decreased. The results from these measurements, as well as the opposite of the correction, obtained by reversing the sign of the ΔK_5 trim of Table XI applied on each corrector while keeping the nominal FiDeL settings unchanged, are shown in Fig. 12.

The newly computed RDT correction does reduce the amplitude of f_{1004} as expected. Simulations were run with decapolar correctors turned off and with the RDT correction applied, using an ac-dipole excitation to obtain the forced RDT. As only the relative response between the two schemes is of interest, field errors are not included in this simulation. While the response of individual decapolar correctors was already validated via chromaticity in Sec. II, this instead validates the combined response of the full correction scheme, all correctors together, on the RDT f_{1004}. An example of the response of the real and imaginary parts of the RDT for these two schemes is shown in Fig. 13 for one arc of the LHC. Both components

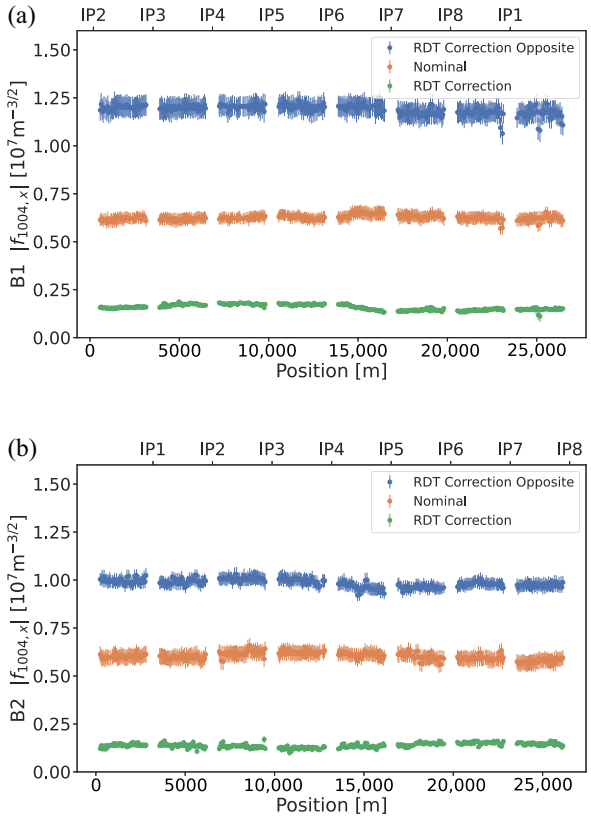


FIG. 12. Measured forced f_{1004} with nominal settings, and combined RDT and Q''' correction with normal and opposite (i.e., sign-reversed ΔK_5) signs. (a) $|f_{1004}|$ for beam 1 (b) $|f_{1004}|$ for beam 2.

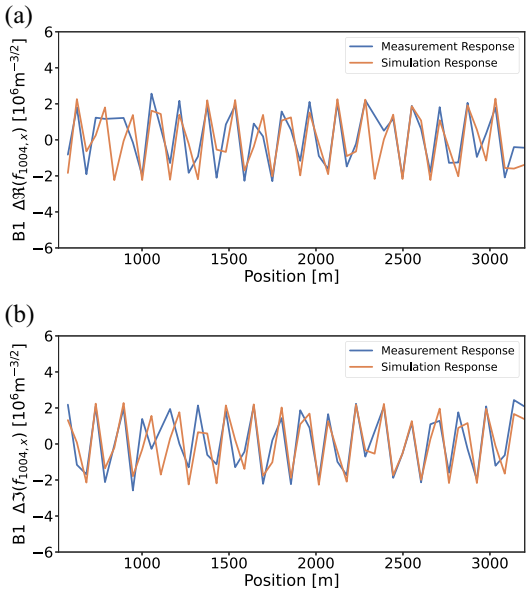


FIG. 13. Comparison between measurement and simulation of the response of the (a) real and (b) imaginary parts of forced f_{1004} upon application of the RDT corrections, on unpowered correctors.

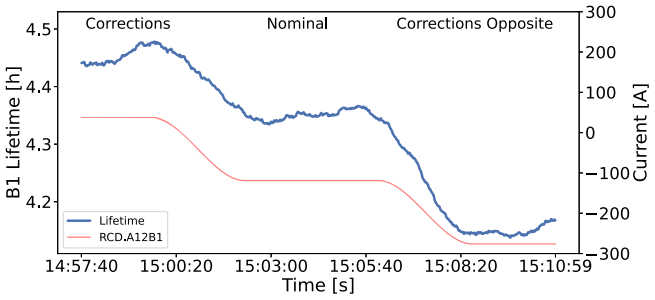


FIG. 14. Measured lifetime of beam 1 with combined corrections of Q''' and f_{1004}, nominal corrections for Q''', and the opposite of the combined corrections.

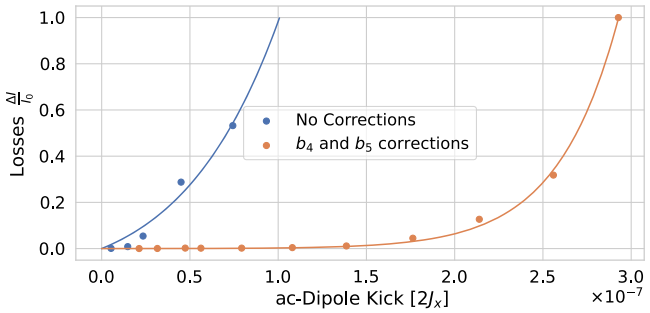


FIG. 15. Relative losses experienced with ac dipole kick amplitude with and without corrections pertaining to Q'', Q''', chromatic amplitude detuning, and f_{1004}.

show the same behavior. The amplitude $|f_{1004}|$ is not used for this comparison, as the real and imaginary parts could be inverted between measurement and simulation while still yielding the same amplitude. The difference between their rms value ratio over the whole ring is ≈6%, indicating that simulations correctly model the decapolar correctors.

The beam lifetime is directly extracted from the logging system, computed from the rate of particle losses measured by the beam loss monitors [43]. In order to understand what can be gained from correcting decapolar fields, a lifetime measurement was taken with the corrections previously described. This scheme corrects the three decapolar observables, being the RDT f_{1004} linked to the resonance $1Q_x - 4Q_y$, the third-order chromaticity Q''' and the chromatic amplitude detuning terms. Figure 14 shows the evolution of the lifetime, starting with corrections applied, removed and then trimmed to their opposite sign. A net change in lifetime for beam 1 can be measured after each application. The acquired signal for beam 2 has been deemed too noisy to be relevant.

As the corrections are adjusted, the beam lifetime responds accordingly. The corrections clearly have a beneficial effect: the lifetime increases by about 3%, while applying the opposite corrections reduces it by about 5%. As lifetime is measured without any ac-dipole excitation, it is a free-motion observable; this improvement is therefore direct experimental evidence that correcting the forced RDT f_{1004} is an effective proxy for correcting the underlying free RDT of the machine, as discussed in the Introduction.

The maximum kick amplitude of the ac dipole corresponds to the largest oscillation amplitude that particles can reach before causing substantial beam losses. Figure 15 shows the relative losses observed for different ac dipole kick amplitudes, both with and without octupolar and decapolar corrections, measured at $Q_x = 0.275$, $Q_y = 0.293$, $Q_{x,\mathrm{ac}} = 0.265$, $Q_{y,\mathrm{ac}} = 0.282$. The results clearly indicate that correcting these fields enhances the forced dynamic aperture [44]. The unique effect of each field can however not be determined as corrections were applied simultaneously.

C. Feed-up contributions

Lower-order multipoles can combine to produce higher-order perturbations affecting the decapole resonances through the BCH expansion. Figure 16 shows an example of one simulated LHC configuration, where various multipole error sources in the main dipole were added to the bare machine, without operational corrections. It is particularly clear that in addition to the decapolar errors, sextupolar and octupolar errors also have the potential to strongly influence the RDT f_{1004}.

The strong potential influence of sextupole and octupole sources on the RDT f_{1004} can be understood, as at the third order of the BCH expansions, sextupoles combine together to create decapolarlike fields, consistent with the analogous derivation of an effective fifth-order resonance term from pure sextupole self-interaction at the Tevatron [45]. This implies that changes in the linear chromaticity Q', through the lattice sextupoles, will affect decapolar observables. Simulations of injection optics with varying Q' show that f_{1004} increases with the chromaticity, confirming the impact of sextupole feed-up, as shown in Fig. 17.

At second order in the BCH expansion, sextupole-octupole combinations also generate decapolarlike terms,

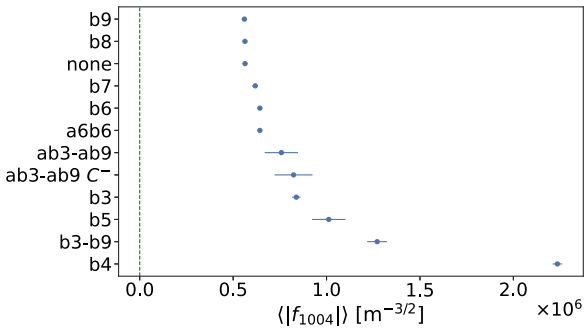


FIG. 16. Simulation of the amplitude of the decapolar RDT f_{1004} depending on the field errors applied on main dipoles as well as coupling (C^-). Sextupolar (b_3) and octupolar (b_4) fields have a clear impact on this amplitude. Main sextupoles are powered in all simulations.

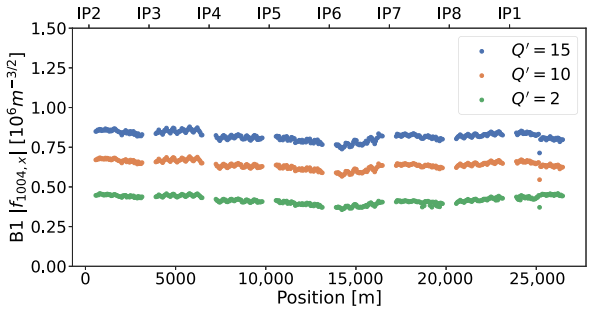


FIG. 17. Simulated change of f_{1004} with varying linear chromaticity Q' generated by sextupoles. Sextupolar combinations increase decapolar RDTs.

as detailed in Sec. 2 of the Appendix. Operational octupoles, including the lattice octupoles used for Landau damping [46], along with operational sextupoles, thus significantly contribute to f_{1004}, whereas octupoles alone do not [13]. Simulations varying lattice octupole strength, while keeping sextupoles nominal, show RDT shifts of almost an order of magnitude, highlighting their dominant feed-up effect, as shown in Fig. 18.

The qualitative behavior predicted by these simulations is also observed experimentally, although via a different octupole circuit: while Fig. 18 varies the lattice Landau octupoles (MO), the measurement below instead varies the octupolar correctors (MCO) used to correct Q''. Measurements of f_{1004} before and after nonlinear chromaticity corrections (Q'' and Q''') revealed an increase in the RDT amplitude, shown in Fig. 19, despite a reduction of the decapolar strength K_5. This is attributed to the powering of octupolar correctors to correct Q'', illustrating the operational relevance of feed-up effects.

Further measurements were performed by varying Q' via lattice sextupoles, shown in Fig. 20. Increasing Q' translated into higher $|f_{1004}|$, consistent with sextupole feed-up, although the measured amplitude was one order of magnitude higher than in simulations, likely due to unmodeled field errors, interactions with octupoles or forced-motion distorted by the ac dipole at high Q' [47].

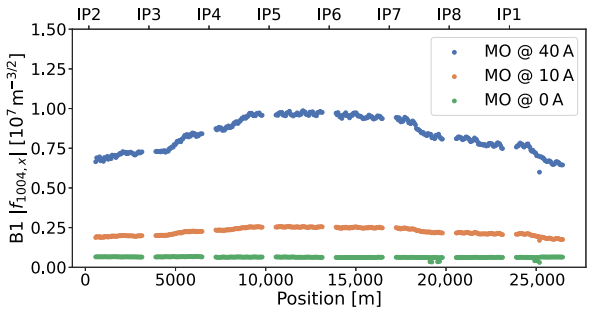


FIG. 18. Simulated f_{1004} depending on the strength of lattice octupoles used for Landau damping.

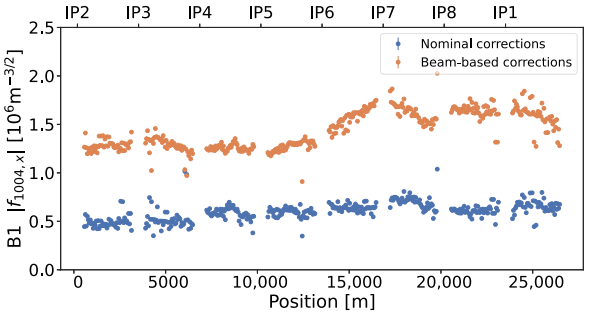


FIG. 19. Increase of the RDT f_{1004} after application of the Q'' and Q''' corrections.

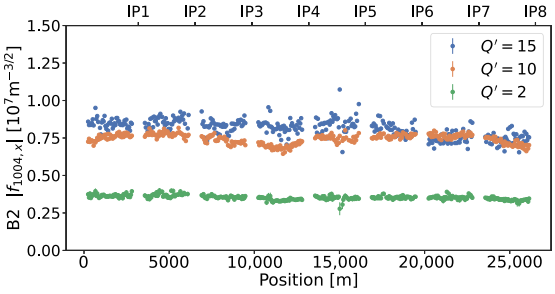


FIG. 20. Measured f_{1004} as a function of linear chromaticity Q' generated by sextupoles.

Additional measurements investigated octupole feed-up using Q'' corrections applied via octupolar correctors, *MCOs*, with various factors. Such corrections use a uniform trim on all correctors of about $\Delta K_4 = 2.5$. The resulting measurements, shown in Fig. 21, demonstrate large changes in the RDT amplitude, confirming the strong effect of octupoles on decapolarlike fields. Further attempts to increase the Q'' corrections were limited by beam losses.

Both sextupole-only and sextupole-octupole feed-up contributions are major sources of decapolar RDTs in the LHC. Theoretical analysis, simulations, and measurements consistently show that operational adjustments to Q' or to the octupole strengths, used for Landau damping, Q'', and amplitude detuning, can significantly alter the

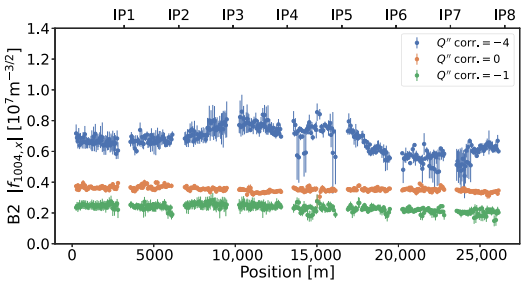


FIG. 21. Shift of f_{1004} with different factors applied to octupolar corrections for Q''.

RDT f_{1004}. These effects must therefore be taken into account in correction and tuning strategies, as doing so could improve both beam lifetime and dynamic aperture, in analogy with the recent optimization of octupolar RDTs in the LHC [48].

D. Replicating the Landau octupoles contribution

As seen previously in Fig. 9, the resonance $1Q_x - 4Q_y$ passes through the beam in tune space, deteriorating the lifetime of the nearby particles. Landau octupoles were shown in Fig. 18 to raise the amplitude of f_{1004} by close to an order of magnitude through feed-up, without any change in the decapolar correctors themselves. In order to isolate and quantify the impact of such an increase of f_{1004} on the beam, independently of its origin, a knob was created that artificially replicates a comparable RDT increase using a purely decapolar source: the current of all decapole correctors in the machine is alternated arc by arc. Such a powering scheme has no impact on chromaticity, as the sum of the strengths K_5 is zero, and only impacts the RDT f_{1004}. It is to be noted that this is not a correction, but purely a way to artificially increase the RDT in order to quantify the effect of the resonance.

Starting with nominal corrections for Q''', a delta of $\Delta K_5 = \pm 10{,}500$ is applied on each decapolar corrector circuit, alternating sign arc by arc. Table XII shows the resulting rms of $|f_{1004}|$ around the ring: the first row ($\Delta K_5 = 0$) is the baseline, with only the nominal Q''' correction applied; the next two rows give the rms obtained for the two opposite arc-by-arc alternating patterns, $\pm 10{,}500$ and its sign-reversed counterpart $\mp 10{,}500$ (i.e., swapping which arcs receive the positive and negative trim). Both patterns increase the rms of $|f_{1004}|$ by more than an order of magnitude relative to the baseline, comparable to the effect of the Landau octupoles, and to a similar degree as each other, confirming that the knob reliably reproduces a large RDT regardless of the specific arc pattern chosen.

In order to measure the lifetime, a long time window is allocated to capture a clean signal, as that returned from monitors can be jittery. The beam lifetime is expressed in hours and decreases over time due to particles being lost. It is adjusted in real-time by the beam loss monitors. Figure 22 shows this lifetime depending on the decapolar strength scheme applied. The current of only one circuit is shown for readability. A current of ≈230 A corresponds to a knob value of $+10{,}500$ K_5 while a current of -45 A corresponds to 0.

TABLE XII. rms of $|f_{1004}|$ relative to the powering scheme of decapolar correctors. The $\pm 10{,}500$ and $\mp 10{,}500$ rows correspond to the two opposite arc-by-arc alternating sign patterns of the artificial knob described in the text.

$\Delta K_5[\mathrm{m}^{-5}]$	rms $\lvert f_{1004}\rvert[\mathrm{m}^{-3/2}]$
0	618,947
$\pm 10{,}500$	17,566,377
$\mp 10{,}500$	17,623,867

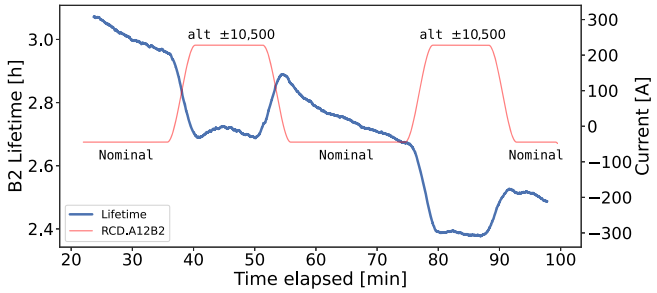


FIG. 22. Measured lifetime of beam 2 upon application of two different powering schemes for decapolar correctors. One trim keeps the RDT f_{1004} at a low amplitude while the other greatly amplifies it.

It is clear from this measurement that a large RDT decreases the lifetime of the beam, more particles being lost. The first pair of trim circuits exhibits an average decrease in beam lifetime of 0.31 ± 0.03 h, while the second pair exhibits a decrease of 0.36 ± 0.03 h. This observed decrease of 20 min accounts for 10% of the beam lifetime at injection energy.

VII. CONCLUSIONS

To better understand the decapolar fields of the LHC, observables such as bare chromaticity and chromatic amplitude detuning were measured for the first time in the LHC. Chromatic amplitude detuning, which accounts for detuning through both horizontal and vertical actions with respect to momentum offset, differs from standard chromaticity in its formulation and provides a more comprehensive view of decapolar errors. This observable was measured for the first time at the LHC. Simulations suggest that the decay of the decapolar component in the main dipoles is the major factor contributing to these discrepancies. This component had previously been neglected in both beam dynamics studies and operational correction strategies. A residual discrepancy remains after accounting for this decay, which is attributed to smaller, unidentified error sources rather than to a single missing component; no dedicated follow-up study is currently planned, as further progress would require a more complete characterization of all magnetic error sources, including their decay, to fully account for the feed-up effects discussed in this paper.

For the first time, measurements and direct corrections of the decapolar RDT f_{1004} were carried out. Further simulations and measurements explored how lower-order multipoles, such as sextupoles and Landau octupoles, can generate decapolarlike perturbations in the beam dynamics via feed-up effects. The findings revealed that these

multipoles, individually or in combination, induce substantial decapolar RDTs during machine operation, which can benefit from active corrections.

Applying combined corrections for third-order chromaticity, chromatic amplitude detuning, and the RDT f_{1004} led to a 3% improvement in beam lifetime. Additionally, intentionally degrading the RDT f_{1004} resulted in a decrease in beam lifetime of about 10%. Furthermore, a significant improvement in the forced dynamic aperture during ac-dipole excitation was observed when corrections were applied.

Initially, the feed-up effect was not well understood, leading to the decision to exclude any decapolar corrections from the machine. However, through studies of decapolar perturbations and the interaction of various multipoles, significant progress was made. The magnetic model for b_5 errors is now more complete, enabling the implementation of these corrections in the machine, which has resulted in both increased lifetime in operation and the possibility of higher-amplitude kicks for nonlinear optics studies. Advancements in understanding the magnetic model and controlling decapolar errors are crucial not only for the HL-LHC but also for future accelerators, which will depend on precise control of high-order nonlinear field errors to optimize dynamic aperture.

ACKNOWLEDGMENTS

The authors would like to thank the LHC machine operators for their support during commissioning and Machine Development time. The authors would also like to thank the LHC optics group for their insights and useful discussions.

DATA AVAILABILITY

There are no publicly available research data or software supporting this manuscript. Requests for further information or data should be sent to the authors.

APPENDIX: TRANSFER MAPS

This appendix is intended to make explicit the higher-order effects created by a combination of magnetic elements. More specifically, decapolarlike fields are created via a combination of sextupoles and octupoles. The case of an array of pure sextupoles generating an effective fifth-order resonance term through self-interaction was similarly derived, using canonical perturbation theory, for the Tevatron in [45]. This section goes more in depth regarding the derivation of their transfer maps.

1. Transfer map of two sextupoles

The transfer map of two sextupoles $H_{3,A}$ and $H_{3,B}$ of strength $K_{3,A}$ and $K_{3,B}$, and lengths L_1 and L_2, separated by a drift to introduce a change of coordinates in $H_{3,A}$ is the following:

$$\mathcal{M} = e^{:Z:} = e^{:H_{3,B}:} \cdot e^{D:H_{3,A}:}. \tag{A1}$$

After such application of the drift on $H_{3,A}$, the two Hamiltonians read,

$$\begin{aligned} H_{3,A} &= \frac{1}{3!} K_{3,A} L_1 \big((L_D p_x + x)^3 \\ &\quad - 3(L_D p_x + x)(L_D p_y + y)^2 \big) \\ H_{3,B} &= \frac{1}{3!} K_{3,B} L_2 (x^3 - 3xy^2). \end{aligned} \tag{A2}$$

Below are detailed each term of the BCH. Each term should be added together in order to obtain the whole effective Hamiltonian Z.

To first order, the following is obtained,

$$\left.\begin{aligned} & K_{3,A} L_1 L_D \begin{pmatrix} \frac{L_D^2 p_x^3}{6} - \frac{L_D^2 p_x p_y^2}{2} + \frac{L_D p_x^2 x}{2} - L_D p_x p_y y \\ - \frac{L_D p_y^2 x}{2} + \frac{p_x x^2}{2} - \frac{p_x y^2}{2} - p_y xy \end{pmatrix} \\ & + K_{3,A} L_1 \left(\frac{x^3}{6} - \frac{xy^2}{2} \right) + K_{3,B} L_2 \left(\frac{x^3}{6} - \frac{xy^2}{2} \right) \end{aligned}\right\} \text{sextupolarlike} \tag{A3}$$

To second order,

$$K_{3,A} K_{3,B} L_1 L_2 L_D \left.\begin{pmatrix} \frac{L_D^2 p_x^2 x^2}{8} - \frac{L_D^2 p_x^2 y^2}{8} + \frac{L_D^2 p_x p_y xy}{2} - \frac{L_D^2 p_y^2 x^2}{8} \\ + \frac{L_D^2 p_y^2 y^2}{8} + \frac{L_D p_x x^3}{4} + \frac{L_D p_x xy^2}{4} + \frac{L_D p_y x^2 y}{4} \\ + \frac{L_D p_y y^3}{4} + \frac{x^4}{8} + \frac{x^2 y^2}{4} + \frac{y^4}{8} \end{pmatrix}\right\} \text{octupolarlike} \tag{A4}$$

And to third order,

$$K_{3,A}^2 K_{3,B} L_1^2 L_2 L_D \left\{ \begin{pmatrix} \frac{L_D^5 p_x^4 x}{48} + \frac{L_D^5 p_x^3 p_y y}{12} - \frac{L_D^5 p_x^2 p_y^2 x}{8} - \frac{L_D^5 p_x p_y^3 y}{12} \\ + \frac{L_D^5 p_y^4 x}{48} + \frac{L_D^4 p_x^3 x^2}{12} + \frac{L_D^4 p_x^3 y^2}{12} - \frac{L_D^4 p_x p_y^2 x^2}{4} \\ - \frac{L_D^4 p_x p_y^2 y^2}{4} + \frac{L_D^3 p_x^2 x^3}{8} + \frac{L_D^3 p_x^2 x y^2}{8} - \frac{L_D^3 p_x p_y x^2 y}{4} \\ - \frac{L_D^3 p_x p_y y^3}{4} - \frac{L_D^3 p_y^2 x^3}{8} - \frac{L_D^3 p_y^2 x y^2}{8} + \frac{L_D^2 p_x x^4}{12} \\ - \frac{L_D^2 p_x y^4}{12} - \frac{L_D^2 p_y x^3 y}{6} - \frac{L_D^2 p_y x y^3}{6} + \frac{L_D x^5}{48} \\ - \frac{L_D x^3 y^2}{24} - \frac{L_D x y^4}{16} \end{pmatrix} \right\} \text{decapolarlike}$$
$$+ K_{3,A} K_{3,B}^2 L_1 L_2^2 L_D \left\{ \begin{pmatrix} \frac{L_D^2 p_x x^4}{48} - \frac{L_D^2 p_x x^2 y^2}{8} + \frac{L_D^2 p_x y^4}{48} + \frac{L_D^2 p_y x^3 y}{12} \\ - \frac{L_D^2 p_y x y^3}{12} + \frac{L_D x^5}{48} - \frac{L_D x^3 y^2}{24} - \frac{L_D x y^4}{16} \end{pmatrix} \right\} \tag{A5}$$

2. Transfer map of a sextupole and octupole

The transfer map of a sextupole H_3 and octupole H_4 of strength K_3 and K_4, separated by a drift like in the previous example is given by

$$\mathcal{M} = e^{:Z:} = e^{:H_4:} \cdot e^{D:H_3:}, \tag{A6}$$

with H_3 and H_4 having as final expressions,

$$\begin{aligned} H_3 &= \frac{1}{3!} K_3 L_1 ((L_D p_x + x)^3 - 3(L_D p_x + x)(L_D p_y + y)^2) \\ H_4 &= \frac{1}{4!} K_4 L_2 (x^4 - 6x^2 y^2 + y^4). \end{aligned} \tag{A7}$$

The first two orders of the BCH of those two elements are given below. To first order, the following is obtained,

$$\begin{aligned} & K_3 \left\{ \begin{pmatrix} \frac{L_D^3 p_x^3}{6} - \frac{L_D^3 p_x p_y^2}{2} + \frac{L_D^2 p_x^2 x}{2} - L_D^2 p_x p_y y - \frac{L_D^2 p_y^2 x}{2} \\ + \frac{L_D p_x x^2}{2} - \frac{L_D p_x y^2}{2} - L_D p_y x y + \frac{x^3}{6} - \frac{x y^2}{2} \end{pmatrix} \right\} \text{sextupolar} \\ & + K_4 \left\{ \left(\frac{x^4}{24} - \frac{x^2 y^2}{4} + \frac{y^4}{24} \right) \right\} \text{octupolar} \end{aligned} \tag{A8}$$

To second order,

$$K_3 K_4 L_D \left\{ \begin{pmatrix} \frac{L_D^2 p_x^2 x^3}{24} - \frac{L_D^2 p_x^2 x y^2}{8} + \frac{L_D^2 p_x p_y x^2 y}{4} - \frac{L_D^2 p_x p_y y^3}{12} \\ - \frac{L_D^2 p_y^2 x^3}{24} + \frac{L_D^2 p_y^2 x y^2}{8} + \frac{L_D p_x x^4}{12} - \frac{L_D p_x y^4}{12} \\ + \frac{L_D p_y x^3 y}{6} + \frac{L_D p_y x y^3}{6} + \frac{x^5}{24} + \frac{x^3 y^2}{12} + \frac{x y^4}{24} \end{pmatrix} \right\} \text{decapolarlike} \tag{A9}$$

[1] O. S. Brüning, J. Poole, P. Collier, P. Lebrun, R. Ostojic, S. Myers, and P. Proudlock, LHC design report, 2004.

[2] E. H. Maclean, F. Schmidt, R. Tomás, R. Bartolini, E. Todesco, R. Steinhagen, G. Vanbavinckhove, and M. Giovannozzi, Non-linear chromaticity studies of the LHC at injection, in *IPAC'11* (JACoW Publishing, San Sebastián, Spain, 2011), pp. 2199–2201.

[3] E. H. Maclean, F. Carlier, J. M. Coello de Portugal, A. Garcia-Tabares, A. S. Langner, L. Malina, T. Persson, P. K. Skowronski, and R. Tomás, Commissioning of non-linear optics in the LHC at injection energy, in *IPAC'16* (JACoW Publishing, Busan, Korea, 2016), pp. 3476–3479.

[4] E. H. Maclean, R. Tomás, F. Schmidt, and T. H. B. Persson, Measurement of nonlinear observables in the

large hadron collider using kicked beams, Phys. Rev. ST Accel. Beams **17**, 081002 (2014).
[5] CERN, FiDeL - the magnetic model of the LHC, https://web.archive.org/web/20220121041323/https://lhc-div-mms.web.cern.ch/tests/MAG/Fidel/, original page (https://lhc-div-mms.web.cern.ch/tests/MAG/Fidel/) no longer resolves; Wayback Machine snapshot cited (2021).
[6] F. S. Carlier, M. Giovannozzi, E. H. Maclean, T. Persson, and R. Tomás, Probing the forced dynamic aperture in the LHC at top energy using AC dipoles, in *Proceedings of IPAC'18, Vancouver, BC, Canada* (JACoW Publishing, Geneva, Switzerland, 2018), pp. 165–168, 10.18429/JACoW-IPAC2018-MOPMF033.
[7] W. Fischer, J. Beebe-Wang, Y. Luo, S. Nemesure, and L. Rajulapati, RHIC proton beam lifetime increase with 10- and 12-pole correctors, in *Proceedings of the First International Particle Accelerator Conference (IPAC'10), Kyoto, Japan* (2010), pp. 4752–4754.
[8] F. Pilat, Y. Luo, N. Malitsky, and V. Ptitsyn, Beam-based Non-linear optics corrections in colliders, in *Proceedings of the 2005 Particle Accelerator Conference* (IEEE, Knoxville, TN, USA, 2005), pp. 601–605.
[9] L. C. Teng, Error analysis for the low beta quadrupoles of the Tevatron collider/location and strengths of correction dipoles in the low beta insertion, Fermilab, Tech. Rep. FERMILAB-TM-1097, 1982.
[10] J. Dilly, V. Ferrentino, M. Le Garrec, E. H. Maclean, L. Malina, T. Persson, T. Pugnat, L. van Riesen-Haupt, F. Soubelet, and R. Tomás, First operational dodecapole correction in the LHC, Phys. Rev. Accel. Beams **26**, 121001 (2023).
[11] E. H. Maclean, F. S. Carlier, J. Dilly, M. Le Garrec, M. Giovannozzi, and R. Tomás, Prospects for beam-based study of dodecapole nonlinearities in the CERN high-luminosity large hadron collider, Eur. Phys. J. Plus **137**, 1249 (2022).
[12] M. Le Garrec, V. Ferrentino, J. Dilly, R. Tomás, K. Paraschou, E. Maclean, and F. Carlier, Measurement and modelling of decapole errors in the LHC from beam-based studies, in *IPAC'23* (JACoW Publishing, Venice, Italy, 2023), pp. 567–570.
[13] M. Le Garrec, LHC effective model for optics corrections : Measurements and corrections of high-order non-linear optics, Ph.D. thesis, Goethe-Universität, 2025.
[14] S. Liuzzo and A. Franchi, Implementation of fully analytic orbit response analysis in python, in *Low Emittance Rings Workshop 2024* (CERN, Geneva, 2024), https://indico.cern.ch/event/1326603/contributions/5773961/.
[15] P. Raimondi, FCC lattice evolution, in *Optics Tuning and Corrections for Future Colliders Workshop* (CERN, Geneva, 2023), https://indico.cern.ch/event/1242395/contributions/5417974/.
[16] Optics tuning and corrections for future colliders workshop, https://indico.cern.ch/event/1242395/timetable/#20230626 (2023).
[17] R. Tomás *et al.*, Towards a high luminosity LHC with even higher performance, in *IPAC'25* (JACoW Publishing, Taipei, Taiwan, 2025), pp. 278–281.
[18] L. Deniau, H. Grote, G. Roy, and F. Schmidt, MAD-X user guide, https://madx.web.cern.ch/releases/last-rel/madxuguide.pdf (2021).
[19] J. Keintzel, L. Malina, and R. Tomás García, Momentum compaction factor measurements in the large hadron collider, in *IPAC'21* (JACoW Publishing, Campinas, SP, Brazil, 2021), pp. 1360–1363.
[20] J. Bengtsson and J. Irwin, Analytical calculations of smear and tune shift, Superconducting Super Collider Laboratory, Dallas, TX, Tech. Rep. SSC-232, 1990.
[21] A. Franchi, Studies and measurements of linear coupling and nonlinearities in hadron circular accelerators Doctoral Thesis, Johann Wolfgang Goethe-Universität, 2006.
[22] E. Forest, *Beam Dynamics: A New Attitude and Framework*, The Physics and Technology of Particle and Photon Beams, Vol. 8 (Harwood Academic, Amsterdam, 1998).
[23] F. Casas and A. Murua, An efficient algorithm for computing the Baker-Campbell-Hausdorff series and some of its applications, J. Math. Phys. **50**, 033513 (2009).
[24] F. S. Carlier, A nonlinear future: Measurements and corrections of nonlinear beam dynamics using forced transverse oscillations, Ph.D. thesis, Universiteit van Amsterdam, 2020.
[25] R. Bartolini and F. Schmidt, Normal form via tracking or beam data, Part. Accel. **59**, 93 (1998); also CERN LHC Project Report 132, 1997.
[26] R. Tomás, Normal form of particle motion under the influence of an ac dipole, Phys. Rev. ST Accel. Beams **5**, 054001 (2002).
[27] R. Bartolini, Resonance driving term experiments: An overview, in *Proceedings of ICAP'06, Chamonix, France* (JACoW, Geneva, Switzerland, 2006), pp. 22–27.
[28] R. Miyamoto, R. Calaga, M. Aiba, R. Tomás, and G. Vanbavinckhove, Measurement of coupling resonance driving terms in the LHC with AC dipoles, in *IPAC'11* (JACoW Publishing, San Sebastián, Spain, 2011), pp. 2067–2069.
[29] S. J. Horney, E. Maclean, P. Burrows, F. Carlier, J. Dilly, L. Deniau, V. Ferrentino, E. Fol, M. Hofer, J. Keintzel, M. Le Garrec, T. Persson, L. van Riesen-Haupt, F. Soubelet, R. Tomás, and A. Wegscheider, Sextupole RDTs in the LHC at injection and in the ramp, in *IPAC'24* (JACoW Publishing, Nashville, Tennessee, USA, 2024), pp. 71–74.
[30] A. Wegscheider and R. Tomás García, Forced coupling resonance driving terms, in *IPAC'21* (JACoW Publishing, Campinas, SP, Brazil, 2021), pp. 3646–3649.
[31] W. Venturini Delsolaro and R. Wolf, Magnetic behavior of LHC superconducting correctors: Issues for machine operation, in *LHC Project Workshop Chamonix XIV* (CERN, Geneva, 2005).
[32] CERN, Ten Out of Ten for LHC Decapole Magnets, CERN, CERN Bulletin BUL-NA-2001-041, 2001.
[33] E. Forest, F. Schmidt, and E. McIntosh, Introduction to the polymorphic tracking code, CERN, SPS and LHC Division Note CERN-SL-2002-044 (AP), 2002.
[34] J. Keintzel, M. Le Garrec, E. Todesco, J. Wenninger, S. Fartoukh, R. Tomás, T. Persson, and M. Solfaroli, 60° phase advance optics measurements in the large hadron collider at CERN, in *IPAC'23* (JACoW Publishing, Venice, Italy, 2023), pp. 571–574.

[35] R. Tomás, S. Fartoukh, and J. Serrano, Reliable operation of the AC dipole in the LHC, CERN, LHC Project Report 1095, 2008.

[36] S. White, E. H. Maclean, and R. Tomás, Direct amplitude detuning measurement with ac dipole, Phys. Rev. ST Accel. Beams **16**, 071002 (2013).

[37] R. Tomás, X. Buffat, S. White, J. Barranco, P. Gonçalves Jorge, and T. Pieloni, Beam-beam amplitude detuning with forced oscillations, Phys. Rev. Accel. Beams **20**, 101002 (2017).

[38] N. Sammut, L. Bottura, and J. Micallef, Mathematical formulation to predict the harmonics of the superconducting large hadron collider magnets, Phys. Rev. ST Accel. Beams **9**, 012402 (2006).

[39] M. Haverkamp, L. Bottura, and M. Schneider, Studies of decay and snapback effects on LHC dipole magnets, in *Proceedings of EUCAS'99*, Sitges, Spain, Inst. Phys. Conf. Ser. 167 (IOP Publishing, Bristol, 1999), pp. 1183–1186; also CERN LHC Project Report 336.

[40] L. Deniau, Magnetic model of main dipoles, CERN, Technology Department EDMS 2458910, 2009.

[41] W. Fischer, A. Jain, and S. Tepikian, Beam-based measurements of persistent current decay in the relativistic heavy ion collider, Phys. Rev. ST Accel. Beams **4**, 041002 (2001).

[42] Y. Papaphilippou, Detecting chaos in particle accelerators through the frequency map analysis method, Chaos **24**, 024412 (2014).

[43] M. Lamont and O. Johnson, LHC beam and luminosity lifetimes revisited, https://cds.cern.ch/record/1967453 (2014).

[44] F. S. Carlier, R. Tomás, E. H. Maclean, and T. H. B. Persson, First experimental demonstration of forced dynamic aperture measurements with LHC ac dipoles, Phys. Rev. Accel. Beams **22**, 031002 (2019).

[45] N. Merminga and K. Ng, Two-fifth resonance islands generated by sextupoles, Fermi National Accelerator Laboratory, Tech. Rep. FERMILAB-FN-0506, 1992.

[46] J. Gareyte, J. P. Koutchouk, and F. Ruggiero, Landau damping, dynamic aperture and octupoles in LHC, CERN, LHC Project Report 91, 1997.

[47] R. Tomás, Adiabaticity of the ramping process of an ac dipole, Phys. Rev. ST Accel. Beams **8**, 024401 (2005).

[48] R. Tomás, F. Carlier, F. Chudoba, L. Deniau, J. Dilly, V. Ferrentino, S. Horney, M. Hostettler, J. Keintzel, S. Kostoglou, M. Le Garrec, E. H. Maclean, T. Nissinen, K. Paraschou, T. Persson, M. Solfaroli, F. Soubelet, A. Wegscheider, and J. Wenninger, Optics for Landau damping with minimized octupolar resonances in the LHC, J. Instrum. **19**, T05010 (2024).